NJC

New Journal of Chemistry

A journal for new directions in chemistry

# Accepted Manuscript

This article can be cited before page numbers have been issued, to do this please use: L. Chen, Q. Kang, Z. Li, B. Zhang, G. Zou and D. Shen, *New J. Chem.*, 2020, DOI: 10.1039/C9NJ05665C.

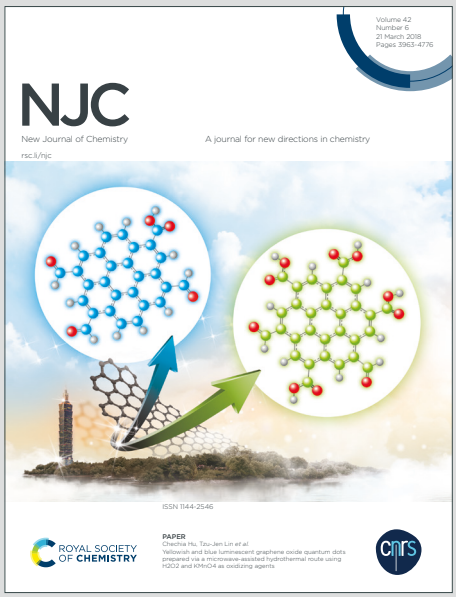




ROYAL SOCIETY OF CHEMISTRY

rsc.li/njc

NJC

View Article Online
DOI: 10.1039/C9NJ05665C

ARTICLE

# Tunable Electrochemiluminescence Properties from Mixed-Monovalent Cations $CsPbBr_3$ Perovskite Nanocrystals

Received 00th January 20xx,
Accepted 00th January 20xx

DOI: 10.1039/x0xx00000x

Lu Chen,[a] Qi Kang,*[a] Zhe Li,[a] Bin Zhang,[b] Guizheng Zou[b] and Dazhong Shen*[a]

Herein we demonstrate a simple approach for tuning the elecrochemiluminescence (ECL) properties of $CsPbBr_3$ perovskite nanocrystals (NCs) by mixed-monovalent cations. By replacing part of $Cs^+$ by $Rb^+$, a series of $Rb_xCs_{1-x}PbBr_3$ NCs were obtained. They exhibit narrow ECL emission peak with the full width at half-maximum about 26~34 nm. After continuously injecting holes to produce different charged state radicals, an annihilation ECL was observed, implying the as-prepared $Rb_xCs_{1-x}PbBr_3$ NCs are in electron-rich state. In the presence of 2-dibutyaminoethanol as co-reactant, strong andodic ECL of $Rb_xCs_{1-x}PbBr_3$ NCs was obtained. From $CsPbBr_3$ NCs to $CsPbBr_3$ NCs, the ECL peak potential position was moved from 1.25 V to 1.80 V with the ECL spectrum peak shifted from 512 to 468 nm, respectively, indicating the tunable ECL properties. The $Rb_{0.2}Cs_{0.8}PbBr_3$ NCs have higher ECL intensity than $CsPbBr_3$ NCs.

## Introduction

Perovskite nanocrystals (NCs) or quantum dots (QDs) have been attracted much attention due to their high photo-luminescence (PL) quantum yield (QY), [1, 2] narrow full width at half-maximum (FWHM),[3] remarkable monochromaticity and wide emission tunability.[4, 5] Among them, all-inorganic lead halide perovskite NCs or QDs, denoted as $ABX_3$ (A is commonly metal cation $Cs^+$, B is usually $Pb^{2+}$, and X is a halogen anion), exhibit high absorption coefficient, long carrier diffusion length and high defect tolerance, which makes them as important materials for optoelectronic devices.[6-8] To obtain better electro-optic properties, the modifications of all-inorganic perovskites with other elements doped or replaced are explored. For example, $Pb^{2+}$ in $ABX_3$ nanocrystals was substituted part or all by other metal ions, such as $Sn^{2+}$,[9] $Mn^{2+}$,[10, 11] $Al^{3+}$,[12] $Bi^{3+}$,[13] $Zn^{2+}$ and $Cd^{2+}$,[14, 15] etc. The effect of monovalent cations exchange on the structure and properties of $CsPbBr_3$ perovskite was also explored. Qiu's group and Chen's group inversitgated the effect of introducing monovalent cation of $Rb^+$ in $CsPbBr_3$ QDs for PL spectrum tuning, and demonstrated that not only the photo energy of $Rb_xCs_{1-x}PbBr_3$ QDs was improved,[16, 17] but the band gap was also changed. Etgar et al investigated the influence of $Rb^+$ substitution on structure stability of $Rb_xCs_{1-x}PbBr_3$ NCs.[18] The $Rb^+$ doped perovskite exhibits enhanced performance in highly efficient light-emitting diodes (LED) and solar cells.[19-21] To our knowledge, the investigation related to the electrochemical properties of $Rb_xCs_{1-x}PbBr_3$ NCs is scarce.

Electrochemiluminescence (ECL) is the smart combination of chemiluminescence and electrochemistry techniques, bringing ECL for various advantages.[22] The generation of ECL is an excitation process, which mainly including the radicals formation processes during the electrochemical reaction and the luminescence produced by the formation of excited state.[23] The ECL emission in the presence of the co-reactant further proves the reliability of the luminescence mechanism. In addition, during the ECL processes, unstable intermediates or reagents can be electrogenerated around electrode surface. As the current and luminescence signals are obtained simultaneously, the luminescence mechanism and electro-chemical reactions of nanomaterials can be investigated conveniently by an ECL method. Bard et al reported for the first time the ECL of silicon NCs in N,N'-dimethylformamide and acetonitrile.[24] Liu and Ju firstly reported the co-reactant anodic ECL of CdTe QDs in aqueous solution at relatively low potential.[25] Ding proved the intermediates of excellent photoelectric material $Au_{38}$ nanoclusters has a short lifetime or low reactivity, because no signal was detected over the potential range of the accessible redox states of the $Au_{38}$ nanoclusters by the annihilation ECL method.[26] Up to now, various QDs have been studied by ECL route, such as CdTe,[27-30] CdSe,[31,32] $MoS_2$,[33] $CuInS_2$[34] and nanoclusters,[26,35,36] 9,10-bis(phenylethynyl)anthracene nanoparticle,[37]and CdS/ZnS QDs coated with polyethyleneimine. [38]

Recently, Huang studied the electrochemical properties of $CsPbBr_3$ NCs, confirmed that the $CsPbBr_3$ NCs can produced

[a.] College of Chemistry, Chemical Engineering and Materials Science, Collaborative Innovation Center of Functionalized Probes for Chemical Imaging in Universities of Shandong, Key Laboratory of Molecular and Nano Probes, Ministry of Education, Shandong Provincial Key Laboratory of Clean Production of Fine Chemicals, Shandong Normal University, Jinan 250014, P. R. China E-mail: kangqi@sdnu.edu.cn (Q. Kang), dzshen@sdnu.edu.cn (D.Shen), Tel.: +86 0531 86180740; fax: +86 053182615258.
[b.] School of Chemistry and Chemical Engineering, Shandong University, Jinan 250100, China.

† Electronic Supplementary Information (ESI) available: TEM images,PL lifetime parameters, XPS spectra, hole injecting ECL transients, influence of scan rate, annihilation ECL profiles of $Rb_xCs_{1-x}PbBr_3$ NCs. See DOI: 10.1039/ x0xx00000x

View Article Online
DOI: 10.1039/C9NJ05665C



ECL of higher color purity than traditional ECL dyes and metal chalcogenide NCs.[39] Herein, the electrochemical redox and charge transfer natures of $Rb_xCs_{1-x}PbBr_3$ NCs were studied by ECL method. By continuously injecting holes or electrons to produce different charged states, the surface charge state and energy route of $Rb_xCs_{1-x}PbBr_3$ NCs were investigated. The influence of the $Rb^+/Cs^+$ ratio on the ECL potential, intensity and spectrum were reported. The tunable ECL properties of the $Rb_xCs_{1-x}PbBr_3$ NCs are helpful to further understand the electro-optic properties of all-inorganic perovskite and to explore their applications.

## Experimental section

**Materials and reagents.** All reagents used were analytical grade. Cesium carbonate (99%), rubidium carbonate (99.8%), lead bromide (99%), 1-octadecene (ODE, >90.0%), oleic acid (OA, AR), oleylamine (OAm, 80–90%), dichloromethane (99.5%), tetrabutylammonium hexafluorophosphate ($TBAPF_6$, 99%), 2-dibutyaminoethanol (DBAE, 99%) and benzoyl peroxide (BPO) were purchased from Aldrich. Toluene was obtained from Sinopharm Chemical Reagent Co., Ltd (Shanghai, China).

**Preparation of Rb/Cs-oleate as precursor.** Rb/Cs-oleate precursor was synthesized according to the method described in ref..[38] with some modifications. Briefly, 1 mmol of $Cs_2CO_3$ and $Rb_2CO_3$ (Rb: Cs = x:1−x, atomic) were added into a 50 mL three-necked flask. Then ODE (16 mL) and OA (1 mL) were injected and mixed adequately. Subsequently, the temperature of the reaction system was risen to 120 °C under stirring and kept at 120 °C for 30 min. Afterwards, the temperature was risen to 150 °C, kept at this temperature until $Cs_2CO_3$ and $Rb_2CO_3$ were dissolved completely. All the processes were carried out under a nitrogen atmosphere.

**Preparation of $Rb_xCs_{1-x}PbBr_3$ NCs.** $Rb_xCs_{1-x}PbBr_3$ NCs were prepared following the previous report.[40] First, ODE (5 mL), OA (0.5 mL), OAm (0.5 mL) and $PbBr_2$ (0.087 g) were loaded into a 50 mL three-necked flask under the nitrogen atmosphere. The mixture was heated to 120 °C under stirring and kept at this temperature for 30 min. After rising temperature to 150 °C, 0.4 mL precursor (Cs/Rb-oleate) solution (preheated to 100 °C) was injected into the flask rapidly. After 5 s, the resulted mixture was cooled in an ice-water bath then was centrifuged at 12000 rpm for 10 min. The precipitated NCs were washed with toluene for three times then ultrasonically dispersed into toluene at the concentration of 40 mg·mL$^{-1}$, and stored in the dark.

**Preparation of $Rb_xCs_{1-x}PbBr_3$ NCs modified electrodes.** The glass carbon electrode (GCE) was polished with a 0.1 μm alumina slurry, and washed with doubly distilled water, and then dried with high-purity nitrogen stream. 5 μL of the $Rb_xCs_{1-x}PbBr_3$ NCs solution (2.5 mg·mL$^{-1}$) was spread on the GCE surface and dried under an infrared lamp to obtain the $Rb_xCs_{1-x}PbBr_3$ NCs|GCE.

**Measurement and characterization.** Transmission electron microscopy (TEM) was conducted with a JEM-1011 electron microscope. PL spectrum was recorded with an F-320 spectrofluorimeter (Tianjin Gangdong Sci. &Tech. Development Co., Ltd., China). UV−Vis absorption spectrum was measured on a TU-1901 spectrophotometer (Beijing Purkinje General Instrument Co., Ltd., China). X-ray diffraction (XRD) patterns were recorded using an X-ray diffractometer (Bruker AXS D8Advance, Germany) with Cu Kα radiation (λ = 1.5418 Å). X-ray photoelectron spectroscopy (XPS) was detected on ESCALAB 250 XPS using monochromatic Al Kα radiation (Thermo Fisher Scientific Co., Ltd., U.S.A.). Differential pulse voltammetry (DPV) was performed using a CHI 822 electrochemical analyzer (Shanghai, China). Cyclic voltammetry (CV) and ECL experiments were recorded with a MPI-EII ECL analyzer (Xi'an Remex Analytical Instrument Co., Ltd, China) with a three-electrode system including a GCE working electrode, a Pt coil as the counter electrode, and an Ag coil as the quasi-reference electrode. The voltage of the photomultiplier tube was biased at 600 V. ECL spectrum was recorded with a homemade ECL spectrum system, which consisted with an Acton SP2300i monochromator, a VersaSTAT 3 analyzer (Princeton Applied Research, USA), a light-tight box, a specially designed light path and a controlling device. The ECL images were obtained from a PyLoN 400BR eXcelon digital CCD camera (Princeton Instruments, USA). A Fourier transform filtering algorithm was used for noise suppression in ECL spectrum by a software of SigmaPlot 7.0.

## Results and discussion

**Characterization of $Rb_xCs_{1-x}PbBr_3$ NCs.** As shown in Figure 1, with increasing Rb content (x), the edge in the absorption spectrum of $Rb_xCs_{1-x}PbBr_3$ NCs was shifted to shorter wavelength region. Similarly, the PL spectra show tunable luminescence emission peaks at 520, 515, 514, 503, 494, 483 and 447 nm at the x values of 0, 0.1, 0.2, 0.4, 0.6, 0.8 and 1 respectively, revealing the quantum confinement effect.[41] The FWHM of the as-prepared $Rb_xCs_{1-x}PbBr_3$ NCs is about 19~28 nm. Under the irradiation of 365 nm UV lamp, bright PL images were visualized (Inserts), with the color changed from green to blue with increasing $Rb^+$ content. These results demonstrate the tunable PL emission of $Rb_xCs_{1-x}PbBr_3$ NCs by adjusting $Rb^+/Cs^+$ ratio. Notably, $Rb_{0.2}Cs_{0.8}PbBr_3$ NCs exhibited highest PL intensity among the $Rb_xCs_{1-x}PbBr_3$ NCs tested. Thus, $Rb_{0.2}Cs_{0.8}PbBr_3$ NCs were investigated mainly in this work.

As can be seen from the TEM image in Figure 2C, the as-prepared $Rb_{0.2}Cs_{0.8}PbBr_3$ NCs exhibit cubic morphologies with an averaged edge length of 10 ± 2 nm. The cubic morphologies may be attributed to the effect of the high synthesis temperature and contribution from the surface energy.[42] It is shown that the size of $Rb_xCs_{1-x}PbBr_3$ NCs is in a reduced trend with the increase of $Rb^+$ content in the range of x=0~0.6 (Figure S1). In the case of x=1, the edges in the cubic morphologies of $RbPbBr_3$ NCs are obscure and the averaged edge length is about 32 ± 4nm. The XRD patterns of $Rb_{0.2}Cs_{0.8}PbBr_3$ NCs are similar with those of $CsPbBr_3$,[40] which

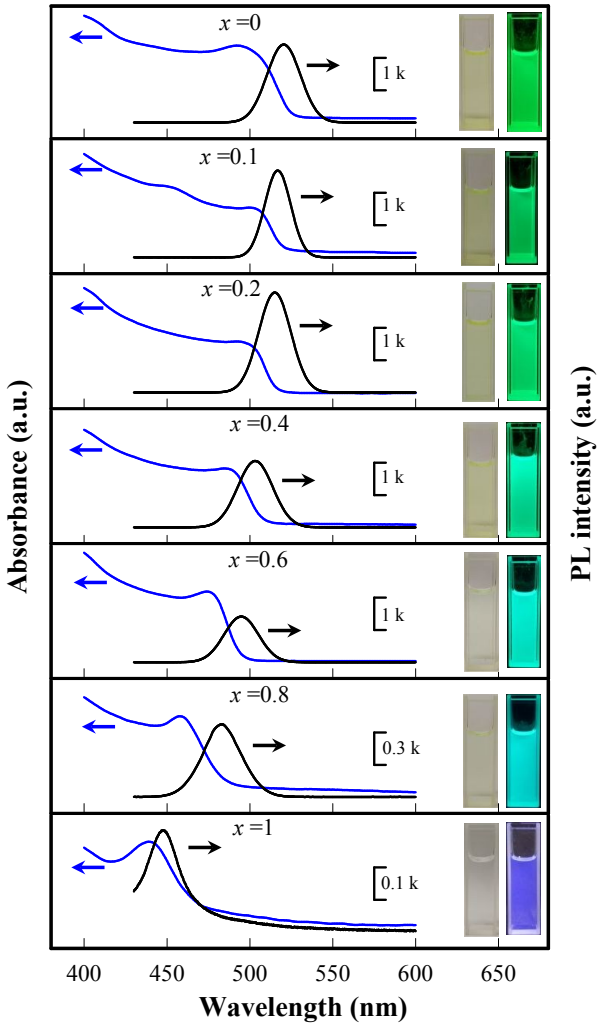


**Figure 1.** Absorption (blue line) and PL spectra ($\lambda_{ex}$: 365 nm, black line) of $Rb_xCs_{1-x}PbBr_3$ NCs. Insert: Photographs of the as-obtained $Rb_xCs_{1-x}PbBr_3$ NCs solutions (left: under ambient light; right: under 365 nm UV light).

were corresponded to the COD ID (5407521) of $CsPbBr_3$ NCs. Due to the smaller ionic radius of $Rb^+$ than $Cs^+$, the replacement of $Cs^+$ by $Rb^+$ leads to crystal lattice contraction and the left shift of characteristic peaks in the XRD patterns, implying that $Rb^+$ has been successful introduced into the $CsPbBr_3$ crystal lattice, which is also supported by the XPS

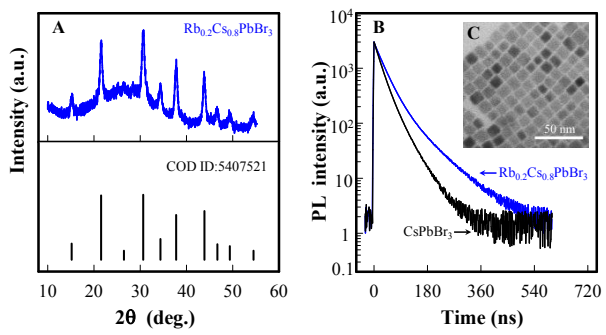


**Figure 2.** (A) X-ray diffraction pattern of $Rb_{0.2}Cs_{0.8}PbBr_3$ NCs ; (B) PL decay curves of $Rb_{0.2}Cs_{0.8}PbBr_3$ NCs and $CsPbBr_3$ NCs; (C) TEM image of $Rb_{0.2}Cs_{0.8}PbBr_3$ NCs.

spectra in Figure S2. In the case of $Rb_{0.2}Cs_{0.8}PbBr_3$ NCs, two additional peaks in $Rb_{0.2}Cs_{0.8}PbBr_3$ NCs appeared at 109.4 eV and 110.8 eV (Figure S2c), which are attributed to the Rb 3d signals, proving that $Rb^+$ ions have been incorporated into $CsPbBr_3$ NCs. The PL decay curves of $CsPbBr_3$ NCs and $Rb_{0.2}Cs_{0.8}PbBr_3$ NCs in Figure 2B were well fitted with a bi-exponential model. The corresponding PL lifetimes were estimated to be 30.9 and 46.8 ns (table S1), respectively. By using quinine sulfate in 0.1 M $H_2SO_4$ (PLQY =54%) as standard reference,[41] the PLQY of $CsPbBr_3$ NCs and $Rb_{0.2}Cs_{0.8}PbBr_3$ NCs were calculated to be 39.6% and 48.1% respectively. The longer lifetime and higher PLQY are responsible for the higher PL intensity in $Rb_{0.2}Cs_{0.8}PbBr_3$ NCs than $CsPbBr_3$ NCs.

**Electrochemical behaviour of $Rb_{0.2}Cs_{0.8}PbBr_3$ NCs|GCE.** As shown in Figure 3, both $Rb_{0.2}Cs_{0.8}PbBr_3$ NCs|GCE and $CsPbBr_3$ NCs|GCE exhibite an obviously enhanced current compared with the background signal in the bare GCE. During the negative initialed potential scan in $N_2$-saturated supporting electrolyte solution, the cathodic DPV profiles display three reduction processes (Figure 3A). The $Rb_{0.2}Cs_{0.8}PbBr_3$ NCs|GCE produced one relative strong reduction peak ($Rex_3$) and two weak reduction peak ($Rex_1$ and $Rex_2$) from -1.60 V to -1.90 V, -0.80 V to -1.0 V, and -1.30 V to -1.50 V respectively, which are similar to those in cathodic DPV of $CsPbBr_3$ NCs|GCE. Therefore, $Rb_{0.2}Cs_{0.8}PbBr_3$ NCs|GCE might be injected with electrons continuously to produce reduced radicals and anions of different charged states, such as $R^-$ ($Rb_{0.2}Cs_{0.8}PbBr_3$ NCs $^-$), $R^{2-}$ ($Rb_{0.2}Cs_{0.8}PbBr_3$ NCs $^{2-}$), and $R^{3-}$ ($Rb_{0.2}Cs_{0.8}PbBr_3$ NCs $^{3-}$).

The anodic DPV profiles in Figure 3B show two similar oxidation processes in both of $CsPbBr_3$ NCs|GCE and $Rb_{0.2}Cs_{0.8}PbBr_3$ NCs|GCE, with the peak potential around 0.82 V ($Ox_1$) and 1.24 V ($Ox_2$). A new oxidation peak of $Ox_3$ was observed around 1.6 V in $Rb_{0.2}Cs_{0.8}PbBr_3$ NCs|GCE, which might be related to the introduction of $Rb^+$ in $Rb_{0.2}Cs_{0.8}PbBr_3$ NCs. In addition, both of the bare GCE and modified GCE display a strong oxidation current ($Ox_0$) from 1.65 V to 1.85 V with a peak position around 1.75 V, indicating that the formation of $Ox_0$ might be attributed to the oxidation of

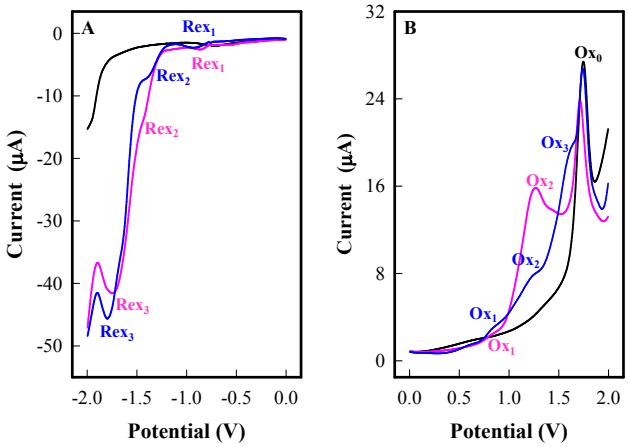


**Figure 3.** Cathodic (A) and anodic (B) DPV profiles of bare GCE (black line), $CsPbBr_3$ NCs|GCE (pink line) and $Rb_{0.2}Cs_{0.8}PbBr_3$ NCs|GCE (blue line) in air-free dichloromethane containing 0.1 M $TBAPF_6$ at 50 mV $s^{-1}$.

View Article Online
DOI: 10.1039/C9NJ05665C



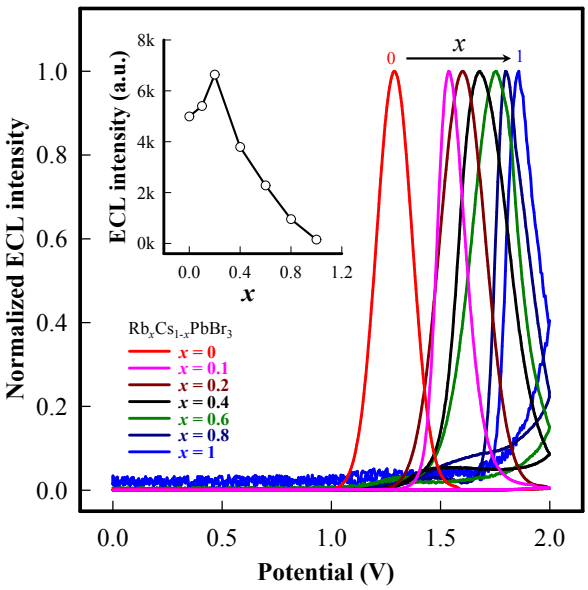


**Figure 4.** Anodic ECL of $Rb_xCs_{1-x}PbBr_3$ NCs|GCE in air-free dichloromethane containing 0.1 M $TBAPF_6$ and 10.0 mM DBAE at 50 mV $s^{-1}$. Inset: ECL peak intensity at different $Rb^+$ content ($x$).

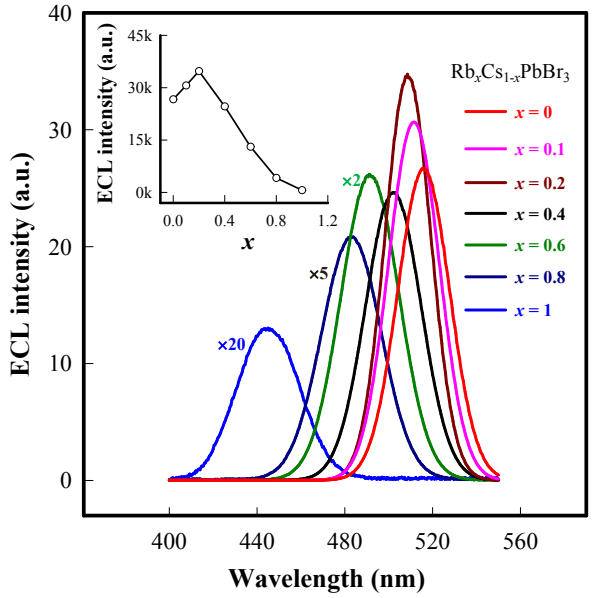


**Figure 5.** Anodic ECL spectra of $Rb_xCs_{1-x}PbBr_3$ NCs|GCE in air-free dichloromethane containing 0.1 M $TBAPF_6$ and 10 mM DBAE by scanning the electrode from 0.0 to 2.0 V at 50 mV $s^{-1}$. Inset: ECL peak intensity at different $Rb^+$ content ($x$).

dichloromethane. Hence, $CsPbBr_3$ NCs and $Rb_{0.2}Cs_{0.8}PbBr_3$ NCs|GCE could be injected with holes continuously to produce oxidized radicals and cations of different charged states, such as $R^+$ ($Rb_{0.2}Cs_{0.8}PbBr_3$ NCs $^+$), $R^{2+}$ ($Rb_{0.2}Cs_{0.8}PbBr_3$ NCs $^{2+}$), and $R^{3+}$ ($Rb_{0.2}Cs_{0.8}PbBr_3$ NCs $^{3+}$).

**Co-reactant ECL of $Rb_xCs_{1-x}PbBr_3$ NCs|GCE.** To further investigate the influence of different $Rb^+$ content on electrochemical properties of $Rb_xCs_{1-x}PbBr_3$ NCs, their ECL behaviors were compared. It is well known that the ECL radiation of NCs can be enhanced significantly in the presence of co-reactant.[31] An effective co-reactant plays an important role in the enhancement of ECL performance. For example, the co-reactant of DBAE has provided a facile strategy for high efficiency ECL of $[Ru(bpy)_3]^{2+}$, which could catalyze the oxidation of amines and enhance the ECL signal.[44] DBAE as a popular co-reactant was also used in the ECL of CdSe/ZnS QDs.[45, 46] In this work, DBAE was selected as anodic co-reactant for $Rb_xCs_{1-x}PbBr_3$ NCs.

Figure 4 displays the anodic ECL performance of a group of $Rb_xCs_{1-x}PbBr_3$ NCs|GCE. In the presence of DBAE, the strong anodic ECL was obtained, indicating that the hole injecting processes and the oxidation effect of co-reactant DBAE. With increasing $Rb^+$ content, the onset potentials and ECL peaks of $Rb_xCs_{1-x}PbBr_3$ NCs|GCE were shifted positively. For example, the ECL peak of $CsPbBr_3$ NCs|GCE around 1.25 V is corresponded to the hole injecting processes of $Ox_2$ for $CsPbBr_3$ NCs. ECL peaks of $Rb_xCs_{1-x}PbBr_3$ NCs|GCE were shifted from 1.56 V to 1.80 V with $Rb^+$ content increased from 0.1 to 0.8. The intensity of the anodic ECL presents an up-and-down trend, with the $Rb_{0.2}Cs_{0.8}PbBr_3$ NCs having the strongest ECL radiation among the series of $Rb_xCs_{1-x}PbBr_3$ NCs tested. These results reveal the tunable performance of primary anodic ECL peak. But in the case of $RbPbBr_3$ NCs|GCE, the anodic ECL intensity is only 3% of that in $CsPbBr_3$ NCs|GCE. The anodic co-reactant ECL for $Rb_xCs_{1-x}PbBr_3$ NCs may be described by the following reaction mechanism.

$$R - e \rightarrow R^+ \quad (1)$$

$$DBAE - e \rightarrow [DBAE^\bullet]^+ \rightarrow DBAE^\bullet \quad (2)$$

$$R + DBAE^\bullet \rightarrow R^- \quad (3)$$

$$R^+ + R^- \rightarrow R^* \quad (4)$$

$$R^* \rightarrow R + h\nu \quad (5)$$

As shown in Figure 5, the anodic ECL emission spectra of $Rb_xCs_{1-x}PbBr_3$ NCs are sharp and symmetrical peaks, especially for $Rb_{0.2}Cs_{0.8}PbBr_3$ NCs. The intensity and potential position of ECL emission peak in $Rb_xCs_{1-x}PbBr_3$ NCs|GCE were related to the content of $Rb^+$ in NCs. Noted that the anodic ECL peaks were almost identical to the PL spectrum of $Rb_xCs_{1-x}PbBr_3$ NCs But the FWHM of ECL spectra is about 3-9 nm wider than that of PL spectra (Figure S3). The wider FWHM in ECL spectra might be attributed to the accumulation of different charges on the excited surface of NCs.[36]

The tunable ECL emission spectra of $Rb_xCs_{1-x}PbBr_3$ NCs via $Rb^+$ content are related to the change in energy band, which is due to effect of particle size and the energy balance within the lattice. As shown in Figure S1, with $Rb^+$ content increasing from x=0 to x=0.6, the size of $Rb_xCs_{1-x}PbBr_3$ NCs is reduced slightly, which results in the blue shift of emission peak in ECL spectra. On the other hand, the introduction of $Rb^+$ into $CsPbBr_3$ NCs changes the electronic dimensionality. Because the ionic radius of $Rb^+$ is smaller than that of $Cs^+$, the hybridization between the $ns^2$ of $Pb^{2+}$ and the $ns^2$ of $Br^-$ orbitals is affected when $Cs^+$ is replaced by $Rb^+$, changing the

View Article Online
DOI: 10.1039/C9NJ05656C

chemical bond between the $Pb^{2+}$ and $Br^{-}$. In 3D original structure of $CsPbBr_3$, the in-plane Pb–Br–Pb band angle is 180°. In the case of $RbPbBr_3$ NCs, the stronger interaction between $Rb^{+}$ and the $[PbBr_6]$ octahedron decreases the in-plane Pb–Br–Pb band angle θ, which increase the band gap.[39] As a result, the ECL emission peak of $RbPbBr_3$ NCs is around 445 nm, which is blue shifted by 70 nm in compared with $CsPbBr_3$ NCs, although the size of $RbPbBr_3$ NCs is even larger than that of $CsPbBr_3$ NCs. Noted that the stability of $RbPbBr_3$ NCs sample is poorer than that $CsPbBr_3$ NCs due to the greater the distortion of the $[PbBr_6]$ octahedron.[18] Consequently, the ECL intensity of $RbPbBr_3$ NCs|GCE is much weaker than that of $CsPbBr_3$ NCs|GCE.

In addition, the cathodic ECL of $Rb_xCs_{1-x}PbBr_3$ NCs|GCE was also measured by using the co-reactant of BPO. Under the experimental conditions, only weak ECL emission was observed (data were not shown).

**Annihilation ECL behaviours of $Rb_xCs_{1-x}PbBr_3$ NCs|GCE.** By switching potential between different oxidization and reduction couples, the annihilation ECL process between the oxidized and reduced states of $Rb_{0.2}Cs_{0.8}PbBr_3$ NCs was studied. The transient ECL behavior of $Rb_{0.2}Cs_{0.8}PbBr_3$ NCs is demonstrated in Figures 6. It can be seen that obvious ECL signals occurred at the first potential stepping from negative potentials (-0.92 V, -1.38 V and -1.80 V) to positive potentials (0.82 V, 1.24 V or 1.6 V), but no annihilation ECL were found at the second potential stepping from positive potentials to negative ones. This result indicates that the transient ECL of $Rb_{0.2}Cs_{0.8}PbBr_3$ NCs|GCE should be obtained by stepping electron injecting process ahead of the hole injecting process. In addition, in the sequential switching from the electron injection to the hole injection, the transient ECL signals were decreased and finally disappeared. It may be attributed to the confined stability of the electrogenerated radicals of $Rb_{0.2}Cs_{0.8}PbBr_3$ NCs. As shown in Figure S4, transient ECL signals in $CsPbBr_3$ NCs|GCE are weaker and decayed more rapidly than $Cs_{0.2}Pb_{0.8}Br_3$ NCs|GCE. One of the possible reasons is that the lifetimes and reactivity of holes injected $Rb_{0.2}Cs_{0.8}PbBr_3$ NCs were more stable than that of $CsPbBr_3$ NCs. On the other hand, electrogenerated anionic or cationic radicals from the $Rb_{0.2}Cs_{0.8}PbBr_3$ NCs may have relative higher stability. The corresponding transient ECL spectra (Insets in Figure 6) displayed single and symmetric peaks at 510 nm with the averaged FWHM of 20 nm, almost synchronized with PL spectra.

The potential scanning rate usually impacts the ECL performance of NCs. Figures S5 shows the influence of scanning rate on the annihilation ECL of NCs|GCE. It can be seen that the strongest ECL of $Rb_{0.2}Cs_{0.8}PbBr_3$ NCs was obtained at 500 mV/s, which was selected as scanning rate of annihilation ECL performance. As can be seen in Figure 7, $CsPbBr_3$ NCs|GCE and $Rb_{0.2}Cs_{0.8}PbBr_3$ NCs|GCE show one strong anodic ECL peak with the potential scanned from 0 to 2 V. The surface of $CsPbBr_3$ NCs and $Rb_xCs_{1-x}PbBr_3$ NCs might be electron-rich states, the anionic free radicals and continuous hole injection generate strong ECL emission in the positive potential scanning process. In the absence of a co-reactant, the ECL signal generated from the NCs might be related to the chemicals on the surface of the electrode or the free radical in

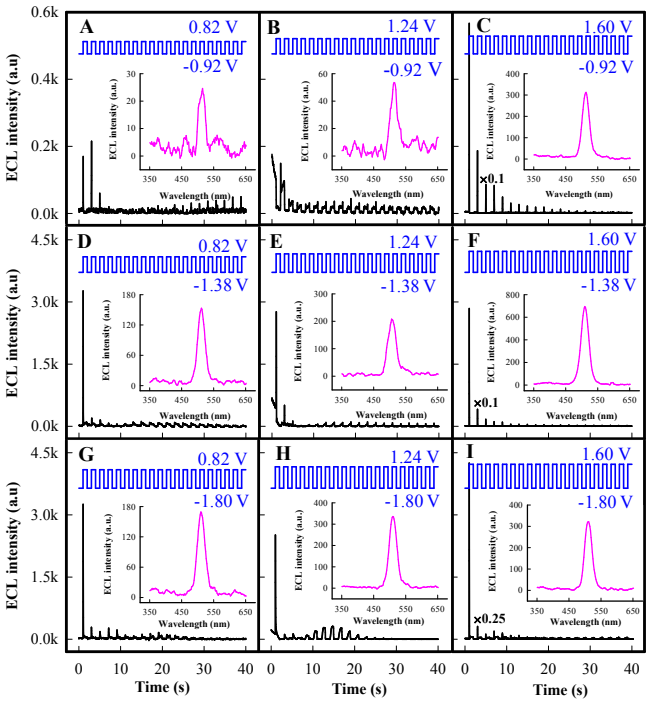


**Figure 6.** Electron injecting initialed ECL transients of $Rb_{0.2}Cs_{0.8}PbBr_3$ NCs|GCE by stepping the potential between (A) -0.92 V and 0.82 V, (B) -0.92 V and 1.24 V, (C) -0.92 V and 1.6 V, (D) -1.38 V and 0.82 V, (E) -1.38 V and 1.24 V, (F) -1.38 V and 1.6 V, (G) -1.8 V and 0.82 V, (H) -1.8 V and 1.24 V, (I) -1.8 V and 1.6 V at 1 Hz for 40 s in air-free dichloromethane containing 0.10 M $TBAPF_6$. The blue lines indicate the applied potential steps. Insets: corresponding ECL spectra of $Rb_{0.2}Cs_{0.8}PbBr_3$ NCs|GCE (pink lines). The exposure time of the CCD was 40 s.

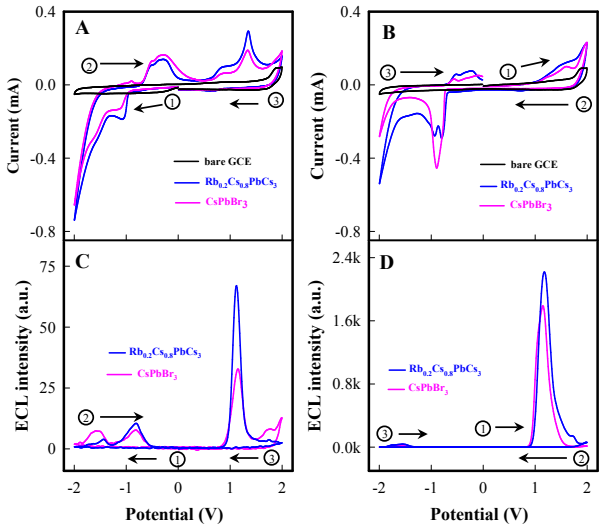


**Figure 7.** CV (A, B) and ECL (C, D) profiles of bare GCE (black line), $CsPbBr_3$ NCs|GCE (pink line) and $Rb_{0.2}Cs_{0.8}PbBr_3$ NCs|GCE (blue line) in air-free dichloromethane containing 0.1mM $TBAPF_6$ with positive or negative started potential scan from 0 V. The scanning rate was 500 mV $s^{-1}$. The arrows indicated the potential scan direction.

the electrolyte solution. It should be noted that the anodic ECL intensity of $CsPbBr_3$ NCs and $Rb_xCs_{1-x}PbBr_3$ is related to their previous surface charge. With the potential scanned initially from 0 to -2.0 V and then from -2.0 to 2.0 V (Figure 7C), the anodic ECL intensity at potential around 1.15V is much weaker than those with potential scanned directly from 0 to 2.0 V (Figure 7D). The reason may be that the initial negative potential scanning results in the inactivation of $CsPbBr_3$ NCs and $Rb_{0.2}Cs_{0.8}PbBr_3$ NCs as well as the accumulation of negative charges on the surface of the electrode. Up injecting hole in the following positive potential scanning, the holes were neutralized firstly with the accumulated negative charges, indicating by the higher anodic currents in Figure 7A. As a result, the amount of holes to excite the anodic ECL of $CsPbBr_3$ and $Rb_{0.2}Cs_{0.8}PbBr_3$ NCs were reduced. When the potential was scanned directly from 0 to 2.0 V, more of the holes were participated in the anodic ECL process. Hence, the anodic ECL intensity in Figure 7D is much higher than that in Figure 7C.

As discussed above, the surface of $Rb_xCs_{1-x}PbBr_3$ NCs is be electron-rich states. Generally, NCs in electron-rich states do not produce strong cathodic ECL without co-reactant. Hence, only weak cathodic ECL emissions were observed in Figures 7C&7D, which is possible due to some impurities in perovskite NCs or supporting electrolyte solutions. As the cathodic ECL signals are very weak, they were not investigated further in this work. As compared in Figure S6, the $Rb_{0.2}Cs_{0.8}PbBr_3$ NCs has more superior annihilation ECL performance than that of $CsPbBr_3$ NCs. When the $Rb^+$ content increased from x=0.2 to x=0.8, the ECL emission became weaker and the peak potential was shifted from 1.2 V to 1.8 V. The lower stability and larger surface defect in $Rb_xCs_{1-x}PbBr_3$ NCs at higher $Rb^+$ content may be the reason of the subdued ECL emission.

## Conclusions

In this work, we have demonstrated the tunable ECL performance of $Rb_xCs_{1-x}PbBr_3$ NCs with by adjusting the $Rb^+/Cs^+$ ratio. The $Rb_xCs_{1-x}PbBr_3$ NCs could be electrochemically injected with holes to produce radicals of different charged states, and then both annihilation and co-reactant ECL were generated. With the increase of $Rb^+$ concentration, the ECL spectra were gradually moved towards the blue light region. The ECL intensity has an up-and-down tendency with the strongest ECL signal was obtained in $Rb_{0.2}Cs_{0.8}PbBr_3$ NCs. The potential position of emission peak is turned from 1.60 V to 1.80 V. The $Rb_{0.2}Cs_{0.8}PbBr_3$ NCs could have superior ECL properties than that from $CsPbBr_3$ NCs. The tunable ECL of $Rb_xCs_{1-x}PbBr_3$ NCs might open up new possibilities to design novel ECL emitters in multiple color ECL analysis and other optoelectronic device applications.

## Conflicts of interest

There are no conflicts to declare.

## Acknowledgements

View Article Online
DOI: 10.1039/C9NJ05665C

This project was supported by the National Natural Science Foundation of China (Grant Nos. 21874083, 21427808), and the Fundamental Research Funds of Shandong University (2018JC017).

## Notes and references

1 X. Li, Y. Wu, S. Zhang, B. Cai, Y. Gu, J. Song and H. Zeng, *Adv. Funct. Mater.*, 2016, **26**, 2435-2445.
2 M. Zhang, Z. Q. Tian, D. L. Zhu, H. He, S. W. Guo, Z. L. Chen and D. W. Pang, *New J. Chem.*, 2018, **42**, 9496-9500.
3 Y. Wang, X. Li, J. Song, L. Xiao, H. Zeng and H. Sun, *Adv. Mater.*, 2015, **27**, 7101-7108.
4 Q. A. Akkerman, V. D'Innocenzo, S. Accornero, A. Scarpellini, A. Petrozza, M. Prato and L. Manna, *J. Am. Chem. Soc.*, 2015, **137**, 10276-10281.
5 G. Nedelcu, L. Protesescu, S. Yakunin, M. I. Bodnarchuk, M. J. Grotevent and M. V. Kovalenko, *Nano Lett.*, 2015, **15**, 5635-5640.
6 N. Yantara, S. Bhaumik, F. Yan, D. Sabba, H. A. Dewi, N. Mathews, P. P. Boix, H. V. Demir and S. Mhaisalkar, *J. Phys. Chem. Lett.*, 2015, **6**, 4360-4364.
7 M. V. Kovalenko, L. Protesescu and M. I. Bodnarchuk, *Science*, 2017, **358**, 745-750.
8 J. J. Ren, X. Dong, G. Y. Zhang, T. R. Li and Y. H. Wang, *New J. Chem.*, 2017, **41**, 13961-13967.
9 T. C. Jellicoe, J. M. Richter, H. F. J. Glass, M. Tabachnyk, R. Brady, S. E. Dutton, A. Rao, R. H. Friend, D. Credgington, N. C. Greenham and M. L. Böhm, *J. Am. Chem. Soc.*, 2016, **138**, 2941-2944.
10 D. Parobek, B. J. Roman, Y. Dong, H. Jin, E. Lee, M. Sheldon and D. H. Son, *Nano Lett.*, 2016, **16**, 7376-7380.
11 D. Chen, G. Fang, X. Chen, L. Lei, J. Zhong, Q. Mao, S. Zhou and J. Li, *J. Mater. Chem. C*, 2018, **6**, 8990-8998.
12 M. Liu, G. Zhong, Y. Yin, J. Miao, K. Li, C. Wang, X. Xu, C. Shen and H. Meng, *Adv. Sci.*, 2017, **4**, 1700335.
13 B. Yang, J. Chen, F. Hong, X. Mao, K. Zheng, S. Yang, Y. Li, T. Pullerits, W. Deng and K. Han, *Angew. Chem., Int. Ed.*, 2017, **56**, 12471-12475.
14 W. Van der Stam, J. J. Geuchies, T. Altantzis, K. H. van den Bos, J. D. Meeldijk, S. Van Aert, S. Bals, D. Vanmaekelbergh and C. de Mello Donega, *J. Am. Chem. Soc.*, 2017, **139**, 4087-4097.
15 M. Aamir, M. D. Khan, M. Sher, N. Revaprasadu, M. A. Malik and J. Akhtar, *New J. Chem.*, 2018, **42**, 17181-17184.
16 H. Wu, Y. Yang, D. Zhou, K. Li, J. Yu, J. Han, Z. Li, Z. Long, J. Ma and J. Qiu, *Nanoscale*, 2018, **10**, 3429-3437.
17 J. W. Xiao, Y. Liang, S. Zhang, Y. Zhao, Y. Li and Q. Chen, *Chem.-Eur. J.*, 2019, **25**, 2597-2603.
18 D. Amgar, T. Binyamin, V. Uvarov and L. Etgar, *Nanoscale*, 2018, **10**, 6060-6068.
19 M. Saliba, T. Matsui, K. Domanski, J. Y. Seo, A. Ummadisingu, S. M. Zakeeruddin, J. P. Correa-Baena, W. R. Tress, A. Abate, A. Hagfeldt and M. Gratzel, *Science*, 2016, **354**, 206-209.
20 Y. F. Shi, J. Xi, T. Lei, F. Yuan, J. F. Dai, C. X. Ran, H. Dong, B. Jiao, X. Hou and Z. X. Wu, *Acs Appl. Mater. Interface*, 2018, **10**, 9849-9857.
21 Y. H. Song, S. H. Choi, W. K. Park, J. S. Yoo, B. K. Kang, S. B. Kwon, H. S. Jung, W. S. Yang and D. H. Yoon, *New J. Chem.*, 2017, **41**, 14076-14079.
22 L. Z. Hu and G. B. Xu, *Chem. Soc. Rev.*, 2010, **39**, 3275-3304.
23 W. Miao, *Chem. Rev.*, 2008, **108**, 2506-2553.

View Article Online
DOI: 10.1039/C9NJ05665C



24 Z. F. Ding, B. M. Quinn, S. K. Haram, L. E. Pell, B. A. Korgel and A. J. Bard, *Science*, 2002, **296**, 1293-1297.
25 X. Liu and H. X. Ju, *Anal. Chem.*, 2008, **80**, 5377-5382.
26 M. Hesari, M. S. Workentin and Z. Ding, *ACS Nano*, 2014, **8**, 8543-8553.
27 Y. Bae, N. Myung and A. J. Bard, *Nano Lett.*, 2004, **4**, 1153-1161.
28 X. Liu, H. Jiang, J. Lei and H. Ju, *Anal. Chem.*, 2007, **79**, 8055-8060.
29 L. Cheng, X. Liu, J. Lei and H. Ju, *Anal. Chem.*, 2010, **82**, 3359-3364.
30 G. Liang, S. Liu, G. Zou and X. Zhang, *Anal. Chem.*, 2012, **84**, 10645-10649.
31 G. Zou and H. Ju, *Anal. Chem.*, 2004, **76**, 6871-6876.
32 X. Zhang, B. Zhang, W. Miao and G. Zou, *Anal. Chem.*, 2016, **88**, 5482-5488.
33 M. Zhao, A. Y. Chen, D. Huang, Y. Q. Chai, Y. Zhuo and R. Yuan, *Anal. Chem.*, 2017, **89**, 8335-8342.
34 X. Long, X. Tan, Y. He and G. Zou, *J. Mater. Chem. C*, 2017, **5**, 12393-12399.
35 K. N. Swanick, M. Hesari, M. S. Workentin and Z. Ding, *J. Am. Chem. Soc.*, 2012, **134**, 15205-15208.
36 H. Jiang, L. Liu and X. Wang, *Nanoscale*, 2017, **9**, 9792-9796.
37 D.B. Xiao, Y.L. Xian, L.L. Liu, Z.J. Gu and B. Wen, New J. Chem., 2014, 38, 902—905.
38 X. Wang, W.P. Deng, L. Shen, M. Yan, S.G. Ge and J.H. Yu, New J. Chem., 2015, 39, 8100—8107.
39 Y. Huang, M. Fang, G. Zou, B. Zhang and H. Wang, *Nanoscale*, 2016, **8**, 18734-18739.
40 L. Protesescu, S. Yakunin, M. I. Bodnarchuk, F. Krieg, R. Caputo, C. H. Hendon, R. X. Yang, A. Walsh and M. V. Kovalenko, *Nano Lett.*, 2015, **15**, 3692-3696.
41 V. I. Klimov, S. A. Ivanov, J. Nanda, M. Achermann, I. Bezel, J. A. McGuire and A. Piryatinski, *Nature*, 2007, **447**, 441.
42 A. Swarnkar, A. R. Marshall, E. M. Sanehira, B. D. Chernomordik, D. T. Moore, J. A. Christians, T. Chakrabarti and J. M. Luther, *Science*, 2016, **354**, 92-95.
43 G.A. Crosby, J.N. Demas, J. Phys. Chem. **75** (1971) 991-1024.
44 X. Liu, L. Shi, W. Niu, H. Li and G. Xu, *Angew. Chem., Int. Ed.*, 2007, **46**, 421-424.
45 S. Wang, E. Harris, J. Shi, A. Chen, S. Parajuli, X. Jing and W. Miao, *Phys. Chem. Chem. Phys.*, 2010, **12**, 10073-10080.
46 T. Hu, X. Liu, S. Liu, Z. Wang and Z. Tang, *Anal. Chem.*, 2014, **86**, 3939-3946.

View Article Online
DOI: 10.1039/C9NJ05665C

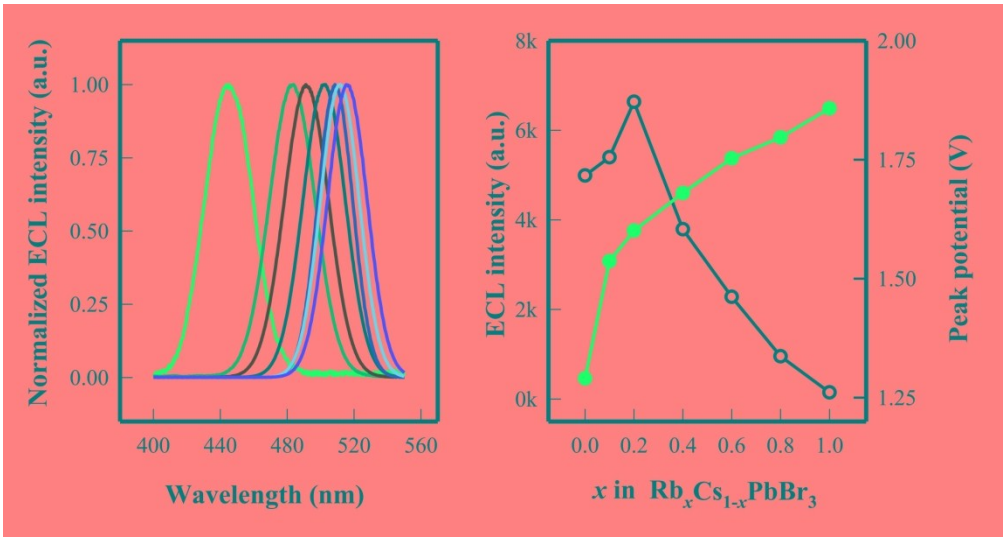


892x475mm (72 x 72 DPI)